Structural monitoring for lifetime extension of offshore wind monopiles: Verification of strain-based load extrapolation algorithm

Lisa Ziegler[a,b,*], Nicolai Cosack[a], Athanasios Kolios[c], Michael Muskulus[b]

[a] Ramboll Wind, 20097 Hamburg, Germany
[b] Department of Civil and Environmental Engineering, Norwegian University of Science and Technology NTNU, 7491 Trondheim, Norway
[c] Naval Architecture, Ocean and Marine Engineering, University of Strathclyde, Glasgow, United Kingdom

[*]Corresponding author: lisaziegler.mail@web.de

Abstract. Lifetime extension needs low-cost assessments that can identify the remaining useful life of offshore wind monopiles. A novel concept for load monitoring was developed that only needs strain gauges installed at one level of the support structure. Damage equivalent loads were calculated from strain measurements and extrapolated along a monopile using a regression algorithm. In this paper, the assumptions behind the load extrapolation algorithm were verified with two consecutive months of measurement data from an offshore wind park. The verification was performed separately for two offshore wind turbines. Both turbines had strain gauges installed at a distance of approximately 15 m and 25 m. Results show that monthly damage equivalent loads can be predicted with errors smaller than 4% based on measurement data only. Prediction using linear regression resulted in similar results for the total fatigue damage as a nonlinear k-nearest neighbor approach, but individual 10-minute damage equivalent loads showed larger differences than for the more robust k-nearest neighbor algorithm, especially for small loads. These results are very promising and should motivate further research.

Keywords: lifetime extension; offshore wind turbine; load monitoring; monopile; strain gauge; fatigue; k-nearest neighbor

1. Introduction

Offshore wind is still a young industry. The majority of assets have been operational for a few years only while the design lifetime of offshore wind turbines and their support structure has been typically 20–25 years in the past. Nowadays, the industry prepares to design new offshore wind farms for a longer lifetime in order to lower the cost of energy. For existing offshore wind farms, extension of the service life is appealing for operators to increase return on investments. Lifetime extension is technically possible if the turbine as well as its support structure have sufficient structural reserves left. Monopiles form the majority of installed support structures today [1] and are subject of this study.

In general, monopiles may have structural reserves at the end of their design life if either loadings are lower or material resistances are higher than designed for. This can be, for example, due to conservatism in environmental parameters (e.g. soil, wind speeds), operational conditions (e.g. turbine downtime), or material properties (e.g. manufacturing tolerances). Technical assessments are necessary to prove that operating assets do not fall below required safety levels during lifetime extensions. According to DNV GL [2], these assessments can be analytical and practical, and/or data-driven. Low-cost solutions for lifetime extension assessments are desirable since it is uncertain beforehand whether a potential for lifetime extension can be confirmed or not.

Analytical assessments are renewed load simulations with updated design models of the wind turbine and support structure as presented by Ziegler and Muskulus [3]. Data gathered during the service life of the offshore wind turbine should be used to update design models as well as environmental and operational assumptions. Practical assessments are inspections on site, which is afflicted with significant costs and risks due to the offshore environment. In addition, Ziegler and Muskulus [4] showed that the probability of detecting decisive fatigue cracks in circumferential welds of monopiles is low. Data-driven assessments may include monitoring of loads or structural health. Load monitoring tracks the load history and enables a direct comparison between design loading and occurred loading to derive the remaining useful lifetime (RUL) of the structure.

Load monitoring of steel structures is established practice for aging infrastructure. As an example, full field strain measurements are applied to evaluate the remaining fatigue life of existing steel bridges by Zhou [5], Leander et al [6], and Frangopol et al [7]. Zhou [5] claims that strain measurements at existing bridges are more accurate for assessing RULs than analytical fatigue assessments, which typically result in overestimation of stress ranges. Leander et al [6] demonstrate how load monitoring with strain gauges can clarify the status in case analytical assessments and inspections yield different results. In the case of a Swedish railway bridge, analytical fatigue reassessments showed that the calculated fatigue life of the stringers was already exceeded while inspections with eddy-current and magnetic particle methods gave no detection of fatigue damage. A monitoring program with strain gauges confirmed the stress ranges calculated in the analytical assessment [6]. Frangopol et al [7] highlight the impact of possible sensor errors associated with electrical strain gauges on fatigue reliability assessments of a steel bridge. Current studies in the field focus on probabilistic fatigue life prediction using strain monitoring data [8] and methods to extrapolate results to structural areas where no sensors are installed [9,10]. In practice, it is not possible to monitor all areas of interest due to cost and access restrictions.

This is particularly relevant for monopiles of offshore wind turbines, for which large parts of the structure are under water and below mudline. It is possible to monitor these areas

directly if the monopile is equipped with strain gauges before pile driving, which has been done in several projects for research and development purposes. Many of these projects, however, experience troubles with the survival rate of the strain gauges during pile driving. For existing assets, it is expensive (below water) or impossible (below mudline) to retrofit strain gauges. Therefore, it would be advantageous to extrapolate measurements from a limited number of sensors to the entire structure. In the offshore wind industry, several researchers have investigated load monitoring strategies with a limited number of sensors using physical models or artificial intelligence. Model-based time-domain approaches include Kalman filters, joint input-state estimation, and modal expansion algorithms [11-13]. These methods aim to track the time history of the vibrations of the whole structure. Artificial intelligence algorithms typically work with 10-minute statistics, such as damage equivalent loads [14,15].

In many existing offshore wind farms, some assets have strain gauges already installed at one height of the structure, typically at the transition piece above water. This data is ready-to-use for lifetime extension assessments at no additional costs. However, these local measurements need to be extrapolated along the entire support structure. In our previous work, we have proposed a novel method for extrapolation of measured loads using a simulation model and statistical algorithm [16]. The method is based on the assumption that a statistical relationship exists between 10-minute damage equivalent loads at two locations, one of which is monitored. The novelty of this work is the verification of this assumption with measurement data. Two months of strain measurements from two elevations at two offshore wind monopiles are used for this purpose. The data was first verified against sensor noise by utilizing that recordings from strain gauges at opposite sides of the circumference of the monopile should mirror each other. Afterwards, one month of data was used for training and the other month of data was used for testing the developed methodology to extrapolate damage equivalent loads along a single monopile, using both linear regression and a nonlinear k-nearest neighbor regression algorithm.

The remainder of the paper is structured as follows: Section 2 describes the load extrapolation algorithm and the measurement data used in the verification study. Results of the verification are discussed in Section 3 and concluded in Section 4.

2. Methodology

2.1. Fatigue loading of offshore wind turbines

Offshore wind turbines operate in a complex environment with wind, waves, current, and various operational conditions. Aero- and hydrodynamic excitation causes long-term cyclic loading at the support structure. The loading history at a specific structural hot spot consists of load ranges with variable amplitudes, each occurring for a specific number of cycles. Cyclic loading restricts the fatigue life of the support structure. The fatigue limit state is often driving the design of monopiles [17].

It is common industry practice to perform fatigue analysis using SN-curves [18,19,20]. SN-curves specify how many load cycles of a specific amplitude a material can endure before failure. The Palmgren-Miner rule of linear damage accumulation is commonly applied to calculate fatigue damage [21]. This hypothesis allows simplifying a variable-amplitude load time series into a single damage equivalent load (DEL). DEL is a load range with constant

amplitude that – when applied for a specific number of reference cycles – causes the same amount of fatigue damage as the original variable-amplitude load time series [15].

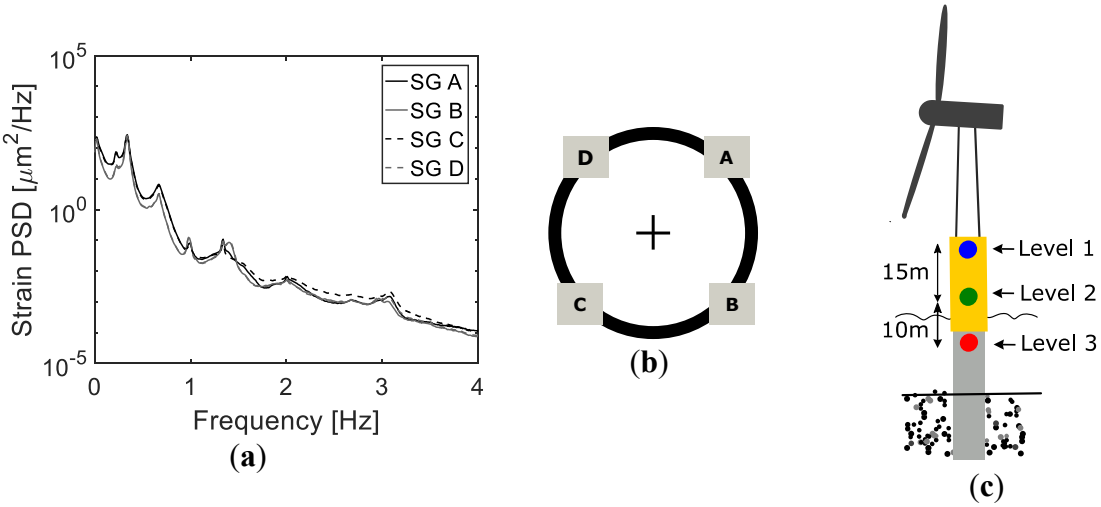

Figure 1. (**a**) Time series of strain measurements from four strain gauges at the transition piece of an offshore wind turbine are transformed into power spectral densities using Fast Fourier transform. **(b)** Four strain gauges are installed at level 1 and 2. They are spaced in 90° intervals. Level 3 only contains strain gauge C and D. **(c)** Schematic position of strain gauges at two offshore wind turbines used for the validation study. At one turbine, the strain gauges are installed at the transition piece at two levels. The distance between the two levels is approximately 15 m. At a second turbine, strain gauges are installed at level 1 and at the upper part of the monopile (level 3). The distance between level 1 and level 3 is approximately 25 m.

2.2. Load extrapolation algorithm

The developed load monitoring concept extrapolates DELs measured with strain gauges at one elevation to another location (or, in principle, along the entire monopile). It utilizes that DELs between different elevations of a structure are correlated through the vibrational modes of the structure. If the structure vibrates in one mode only, DELs at different elevations of the structure will be highly correlated.

Figure 1 (a) shows power spectral densities of strain measurements at the transition piece of an offshore wind turbine. Excitation frequencies are quasi-static contributions from wind forces, wave excitation, first fore-aft and side-side bending frequencies, rotational blade-passing frequencies (1P and 3P), and the second fore-aft and side-side bending frequencies. Consequently, for each DEL measured at one elevation, a range of DELs at another elevation can occur depending on how the structure vibrates. Ziegler et al [16] showed that this range of DELs has a well-defined lower bound with limited scatter for a monopile support structure. This allows the application of a statistical model to predict DELs at a lower elevation, such as near or below mudline (where it is difficult to place and maintain strain gauges), from measurements at a higher elevation, such as the transition piece.

The extrapolation can be performed either based on data or based on simulations. Data-based extrapolation requires that strain measurements were performed at all elevations of interest for a representative period of time. This data can be used to train the extrapolation

algorithm for future use once measurements at one of the elevations are terminated. If strain measurements were never taken at an elevation of interest, it is required to train the extrapolation algorithm with data from numerical analysis. This paper presents results for the data-based extrapolation approach, with the aim of verifying it in a limited setting (between only two locations and with only two months of data), but we mention and discuss the simulation-based approach also, for completeness. The methodology for both approaches is visualized in Figure 2 and summarized in the following. The reader is referred to [16] for further details.

A. *Measurements:* Bending strain is measured at elevations 1,…,n of the monopile through adequately installed sensors. An example of sensor types and placement is given in Section 2.3. In addition, recordings from operational and environmental conditions (such as from SCADA, wave buoys, met masts, etc.) are optional to use in the load extrapolation concept.

B. *Data processing:* The measured strains ε are transformed into bending moments M according to Equation 1. E is the Young's modulus and Z is the elastic section modulus.

$$M = E \cdot Z \cdot \varepsilon \tag{1}$$

The time series are then split into 10-minute intervals. Rainflow counting is performed on each time series to obtain the load ranges S_i and corresponding number of cycles N_i [20]. Results are transformed into measured DELs with Equation 2. N_k is the number of reference cycles, m is the inverse slope of the considered SN-curve, and n is the number of load ranges.

$$DEL = \left(\sum_{i=1}^{n} \frac{N_i}{N_k} S_i^m \right)^{\frac{1}{m}} \tag{2}$$

C. *Numerical analysis:* In the simulation-based approach, aero-hydro-servo-elastic simulations are performed with a finite element model that represents the global dynamic behavior of the installed offshore wind turbine. The finite element model used in design should be updated with on-site measurements to ensure that modal properties (such as natural frequencies, mode shapes, and damping) are represented correctly. This is typically an iterative process that tries to minimize the error between simulated and measured responses, e.g., using a gradient-based optimization algorithm.

Realistic environmental and operational conditions as input for the load simulations are assembled into load cases. Sources for information on realistic conditions are on-site measurements (e.g. wave buoy, met mast), recordings from the turbine control and performance monitoring system (SCADA), and site assessments during design. For each load case, aero-hydro-servo-elastic simulations in line with design requirements and current state-of-art should be performed [22].

10-minute time series of loads at specified elevations are obtained from the simulations for each load case. The elevations are the point at the structure where sensors are installed (*elevation 1,…,n*), and the desired elevation to extrapolate to (*elevation n+1,…,z*). Rainflow counting is performed and DELs are obtained for each 10-minute time interval.

Figure 2. Methodology of strain-based load extrapolation algorithm.

D. *Extrapolation:* The methodology to extrapolate DELs is similar for the data-based and the simulation-based approach. First, a reference elevation, which is continuously equipped with strain gauges, and an elevation to extrapolate to, is chosen. If historical strain measurements for the extrapolation elevation exist, data-based extrapolation (D1) can be performed. Otherwise, simulation-based extrapolation (D2) must be applied.

   DELs (measured or simulated) from both elevations are now assembled into pairs. These joint measurements form the data basis for extrapolation. A simple approach to relate the values at the reference elevation with the values at the extrapolation elevation is linear regression. We will see below that this can result in an accurate estimate of the total damage incurred.

   However, a disadvantage of linear regression is that it cannot accurately capture nonlinear relationship between the two variables of interest (DEL at reference elevation and DEL at extrapolation elevation). We therefore proposed an alternative, more robust nonlinear regression algorithm in [16] that is shortly explained here: DELs are sorted ascending for the reference elevation. Each DEL at the reference elevation has a corresponding DEL at the extrapolation elevation. These either occur at the same time (in case of measurements) or for the same input conditions (in terms of load cases used in simulations). The sorting order from the DELs at the reference elevation is applied to the DELs of the extrapolation elevation also. This results in the data basis for extrapolation, namely a row of ascending DELs from the reference elevation each having a corresponding DEL at the extrapolation elevation.

   Once a new DEL is measured at the reference elevation, it is sorted into the ascending array of DELs from the data basis for extrapolation. A number of neighbors of DELs from the data basis and the corresponding DEL pairs at the extrapolation elevation are chosen. The choice purely depends on the absolute value of DEL; underlying environmental and operational conditions are ignored. This assumes that loading conditions do not affect the extrapolation or more specifically, that deviations average out over time (i.e., among the set of different loading conditions occurring in the period of interest) without a systematic bias. The DEL at the extrapolation elevation is predicted as the mean (or weighted mean) from the chosen, neighboring DELs of the data basis. This is an application of the k-nearest neighbor regression algorithm.

   The selection of neighbors can be altered if information on operational or environmental parameters is available, e.g. from the SCADA system. Only neighbors with similar input conditions are then considered for the extrapolation.

   We remark that the extrapolation in step D can also be performed with other algorithms, but the k-nearest neighbor regression algorithm is conceptually simple, easy to implement, and has been found to result in relatively accurate results. Therefore, the results presented in this paper focus on the k-nearest neighbor regression algorithm.

2.3. Measurement data

In this paper, we analyzed measurement data from two offshore wind turbines on monopile foundations. Both are situated in the same wind farm and are standard variable-speed, pitch-controlled wind turbines. The location of the wind farm is a typical North Sea site with medium-range water depth. Both turbines were exposed to similar environmental conditions with less than 3 m difference in water depth. Two months of measurement data

were available for both offshore wind turbines. The months were consecutive in the year and had similar operational conditions. Wave conditions during the measurement period were somewhat more benign than design conditions. The mean significant wave height was approximately 30% lower than the mean calculated from scatter diagrams used in fatigue assessments during design of the monopile. However, the mean peak periods, important for fatigue due to possible resonant excitations, differed only by 4% between the measurement period and the design basis. Further information on the type of wind turbines and site are excluded for confidentiality purposes.

The wind turbines are equipped with the following sensor system:

- At the **first turbine**, electrical resistance strain gauges were installed at the transition piece of the support structure at two different heights. The distance between the two levels is approximately 15 m. Figure 1 (c) shows the approximate position of the two sets of strain gauges at level 1 and level 2. On each level, four axial strain gauges are placed with 90° spacing around the circumference of the transition piece. The setup is redundant which makes it possible to detect calibration errors and to identify the amount of noise in the measurements. Figure 1 (b) shows spacing and labeling of the strain gauges.
- The **second turbine** has electrical resistance strain gauges at the upper part of the transition piece (level 1) and upper part of the monopile below water (level 3). The distance between both levels is approximately 25 m. The elevation of the strain gauges is illustrated in Figure 1 (c). On level 1, four axial strain gauges are placed similar to turbine 1. On level 3, only two axial strain gauges are placed at position C and D.
- The strain gauges were calibrated and compensated for temperature effects. The sampling resolution was 20 Hz.
- 10-minute average values of power output, turbine status, yaw direction, and mean wind speed from the nacelle anemometer were obtained from the SCADA system.

2.4. Verification study

The data-based load extrapolation algorithm is verified with strain gauge data obtained from two offshore wind turbines as described in the previous sections. One month of the data was used to train the extrapolation algorithm (training data set). The performance of the algorithm was then tested with data from the second month (testing data set). Consequently, no aero-hydro-servo-elastic simulations have been performed in this work. The simulation-based extrapolation (cf. Figure 1) shall be addressed in future work.

Three validation studies were performed for turbine 1; two studies for turbine 2. The validation studies are shown in Table 1. In **case 1**, the complete data set of DELs was used for the extrapolation. This includes all time periods for which strain measurements were uninterrupted during 10-minute intervals and time-synchronized SCADA data was available. In **case 2**, the extrapolation was performed conditional on power production recorded by the SCADA system. The algorithm was trained to distinguish between DELs recorded in three operational states: idling (mean produced power ≤ 0 kW), rated power (mean produced power $\geq$ rated power), and the remaining conditions. For **case 3**, the data set was cleaned by utilizing the redundancy of the sensor layout of turbine 1. Time series from strain gauges at opposite sides of the transition piece (A-C and B-D) should mirror each other. Therefore, the same DEL should be obtained from both sensors under ideal conditions. The difference between

DELs from opposing strain gauges was evaluated to obtain an estimate of the noise level of the measurements. In the cleaned data set, only 95% of the DELs were further processed in the validation study. 5% of the DELs with the largest differences between opposing strain gauges were deleted from the data set.

Table 1. Validation studies of the load extrapolation algorithm performed for turbine 1 and turbine 2.

Case	Description	Turbine 1	Turbine 2
1	Extrapolation of DELs	X	X
2	Extrapolation of DELs with filter for power production	X	X
3	Extrapolation of DELs with cleaned data set	X	

3. Results and discussion

3.1. Data processing

The measured data was checked for measurement noise and plausibility. Figure 3 (a) presents the time series of raw strain data of turbine 1 from the strain gauges B and D during one day. The time series show an opposing behavior. Figure 3 (b) shows the DELs obtained from the time series in Figure 3 (a) after rainflow counting. The DELs show a good match with a mean absolute percentage error of 3.0% for this day. This indicates that the sensors perform well with little measurement noise. The DELs measured by strain gauge D are slightly higher than from strain gauge B indicating small gain differences in the calibration of both strain gauges. Figure 4 (a) shows the difference between strain gauges B and D for the two measurement elevations at the transition piece for one month. The differences between the strain gauge at the upper elevation are higher than for the lower elevation. On average, the differences are below zero at both levels, which indicates that there is a small gain error in the calibration in line with Figure 3 (b). Note that the figures show normalized data (due to confidentiality reasons), whereas all analyses were performed with non-normalized data.

In Figure 4 (b) the measured mean fore-aft bending moment from 10-minute time intervals is plotted as a function of mean wind speed from the SCADA system. The data was selected so that the turbine rotor is facing in approximately the same direction as the strain gauge. For this example, the strain gauge is located at 315°. All data points where the yaw direction of the turbine lies between 305° and 325° are included in the plot. The mean bending moments at the height of the strain gauge resulting from a theoretical thrust curve are plotted as a black line in the same figure. The theoretical thrust curve was estimated from typical thrust coefficients for a turbine of that size and from basic geometry, since no detailed information on thrust was available. The measurements follow the shape of the calculated bending moment due to thrust, thus it is concluded that the data is plausible to use for the validation study. Bending moments at wind speeds below 4 m/s are higher than the theoretical value, possibly due to turbulence, inaccuracy of wind speed measurements from the nacelle anemometer, or potential offsets in the calibration of the strain gauge.

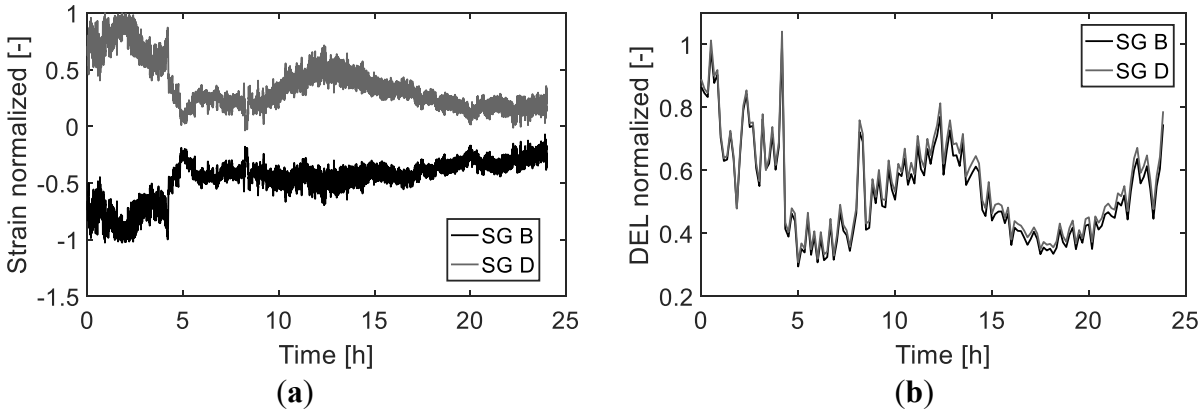

Figure 3. Strain gauge (SG) data from turbine 1. The data is normalized to the maximum of the time series. **(a)** 24 hours of measurements from strain gauges at opposite positions of the circumferential of the transition piece. **(b)** 10-minute DELs from opposing strain gauges after rainflow counting. The difference between the DELs from the two strain gauges is small.

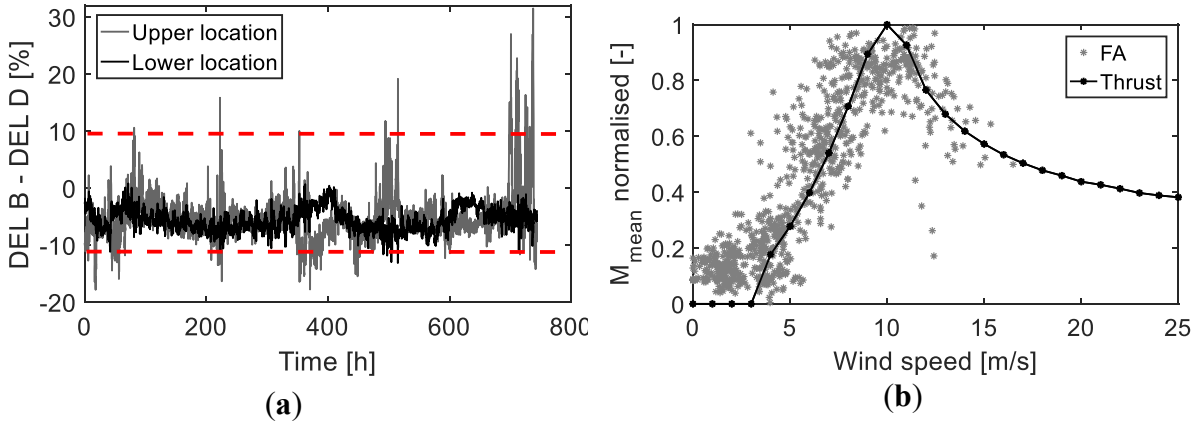

Figure 4. (a) Difference of DELs obtained from opposing strain gauges B and D of turbine 1 during one month in percent. The differences are normalized to the value of DEL B at the respective elevation. Only 95% of the DELs with the lowest differences between opposing strain gauges were considered in the cleaned data set. This corresponds to a threshold value of ±10.3% (red line). **(b)** Mean fore-aft (FA) bending moment (grey dots) from 10-minute time intervals as a function of wind speed. The calculated bending moments from a theoretical thrust curve of the turbine (black line) were estimated from turbine size and basic geometries. All data was normalized to the maximum of the theoretical thrust curve.

Table 2. Sizes of data set used in validation study. The cleaned data set is shown in brackets.

	Turbine 1		Turbine 2	
	Month 1	**Month 2**	**Month 1**	**Month 2**
No. of DELs	4453 (4230)	4214 (4003)	4226	4115
Data availability	99.8% (94.8%)	97.6% (92.6%)	94.7%	95.3%
Max. deviation	39.0% (10.3%)	855.9% (11.5%)	--	--

Table 2 shows the size of the data sets used in the validation study. Ideally, a month with 31/30 days should have 4464/4320 DELs recorded. The uncleaned data set of both turbines is smaller due to interruptions of strain measurements or missing SCADA data. The data availability of the uncleaned data set is above 94% for both turbines. The maximum differences between DELs from opposing strain gauges in the uncleaned data set were 39.0% and 855.9%. The large difference of 855.9% belongs to a DEL that is very small (<0.05 MPa), therefore the impact of sensor noise is large. For case 3 of the validation study (cf. Table 1), 5% of the DELs which have the highest differences were excluded from the data set. This corresponds to a threshold value of ±10.3% differences between DEL B and DEL D that is allowed in the data set for this month. The threshold value is marked by broken red lines in Figure 4 (a). This final data set used in the study is shown in Table 2. Only the data set for turbine 1 was cleaned since turbine 2 did not have opposing strain gauges for comparison.

3.2. Data-based extrapolation

Figure 5 (a) shows two months of DELs from turbine 1 for the two measurement elevations. DELs were sorted in ascending order for the upper measurement elevation (grey dots), thereby discarding the information about the time of occurrence. The corresponding time stamp when these DELs occur was indexed. The index was then used to sort the DELs from the lower measurement elevation in the same order (black dots), such that corresponding DELs appear at the same horizontal position. The lower elevation is approximately 15 m below the upper elevation.

In Figure 5 (b) DELs are colored that correspond to idling and rated power conditions. Idling DELs were selected by filtering SCADA data for entries where power output is zero (black dots). The mean wind speed of these 10-minute time intervals is below the cut-in wind speed of the turbine. Rated power DELs were filtered from SCADA also (red dots). All remaining data points (grey dots) correspond to mean wind speeds between cut-in wind speed and rated wind speed of the turbine. Both rated power and idling conditions show less scatter than the remaining data points.

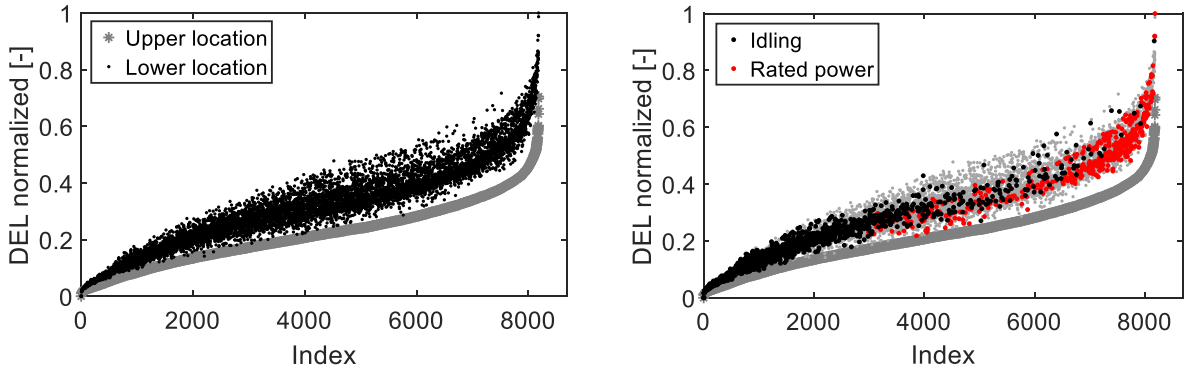

Figure 5. (a) Measured DELs at two elevations of the structure of turbine 1 during two months. DELs are normalized to the maximum of the lower elevation. **(b)** DELs where the turbine 1 produces rated power are colored in red. The black colored DELs are idling conditions where the power output is zero and the average wind speed is below cut-in wind speed of the turbine. The remaining grey dots correspond to mean wind speeds between cut-in and rated wind speed.

3.3.1. Results with linear regression

Before testing the nonlinear k-nearest neighbor algorithm a linear regression analysis was performed. Figure 6 (a) shows scatterplots of the DELs for both months at the two elevations for Turbine 1, illustrating the joint distribution of the measurements. The values from both locations are strongly correlated with an R^2 variance score of 0.96, for both months. Between the two months, the maximum DEL value differed by less than 2%, and the standard deviation of the DELs differed by less than 28%, with slightly higher values for location 2 than for location 1. The ratio between predicted and actual DELs was up to 2.24 (month *M1*) and 1.75 (month *M2*), respectively, with a mean of 1.03 (month *M1*) and 0.98 (month *M2*). The highest relative differences were observed for the lowest DEL values.

All 10-minute DELs were combined into a monthly DEL ratio using Equation 3. The ratio between predicted and measured total DEL for month *M1* is 0.99; for prediction of month *M2*, using the regression line estimated for month *M1*, it is 0.95. The ratio between predicted and measured accumulated damage (taking the exponent *m* in Equation 3) was 0.97 (Month M1) and 0.82 (Month *M2*), respectively. Although the total damage could be predicted very well within the training month, the prediction deteriorated for the test month. This is not surprising, as the true regression line for month M2 had a somewhat different slope than the regression line for month M1.

$$DEL_{month} = \left(\sum_{i=1}^{k} DEL_i^m \right)^{\frac{1}{m}} \quad (3)$$

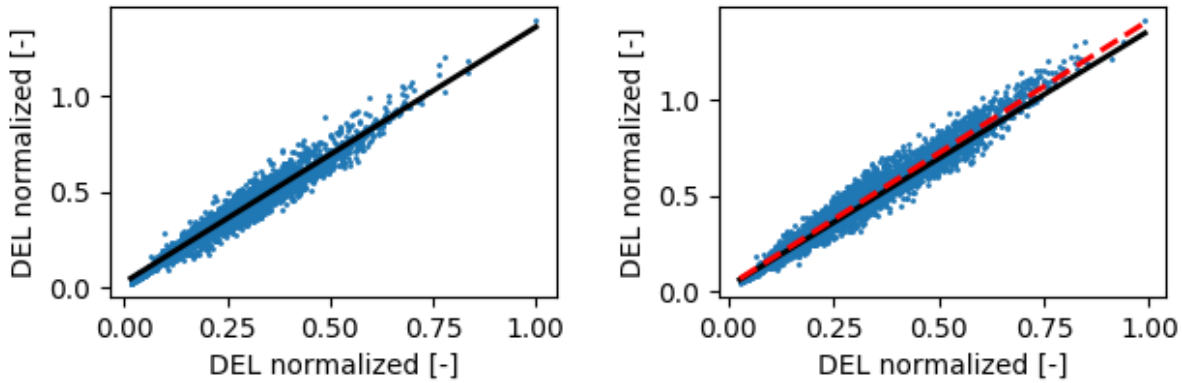

Figure 6. (a) Scatterplot of DELs at the two locations at Turbine 1 for Month 1. The values are shown normalized with respect to the largest DEL at location 1 (for confidentiality reasons). The least squares linear regression results in the bold line. **(b)** Scatterplot of DELs at the two locations at Turbine 1 for Month 2. The values are shown normalized with respect to the largest DEL at location 1 in Month 1. The bold regression line is the same as for Month 1, as it is used for predictions. The broken line (in red) shows the actual linear regression line for Month 2.

3.3.2. Results with nonlinear k-nearest neighbour regression

Figure 7 (a) compares measured DELs and extrapolated DELs for turbine 1 (case 1) where the algorithm was trained with month *M1* (training data set) and tested with month *M2* (testing data set) for one neighbor (red dots) and fifteen neighbors (light grey dots). The more neighbors are chosen, the more is the prediction smoothed in comparison to the scatter of the measurements.

In Figure 7 (b) the histogram of the extrapolation results is shown for case 1. The algorithm was first trained with month *M1* (training data set) to predict month *M2* (testing data set). Afterwards, it was trained with month *M2* to predict month *M1*. There is a difference of up to 40% between predicted and measured 10-min DELs, much less than with the linear regression (up to 75%, not shown). All 10-minute DELs were combined into a monthly DEL ratio using Equation 3 again. The cumulative ratio between predicted and measured DELs for month *M1* is 1.04; for prediction of month *M2* it is 0.96.

Figure 8 shows the monthly prediction errors in terms of cumulative DELs and damage for turbine 1 (a) and turbine 2 (b) for each case. The prediction error of damage is larger since it is exponentiated with the material parameter *m* of the corresponding fatigue stress cycle curve (SN-curve). For turbine 1, the changes in prediction errors with the cleaned data set (case 3) were minor compared to the full data set (case 1). In addition, filtering for power production (case 2) yields comparable results to the unconditional extrapolation. This is possibly due to a counteracting effect: The filter reduces the scatter of DELs at the lower elevation, which is expected to improve the prediction. On the other hand, the prediction accuracy decreases with less data points available. The filter reduces the amount of data points in each category, which might counteract a potential improvement of the prediction due to the reduction of scatter. For turbine 2, the DEL prediction error of month M1 improves from -2.7% to -2.0% while it does increase from -0.4% to 0.9% for month M2 when filtering is applied. In line with turbine 1,

the effect of filtering was small in this case study. The influence of filters may be better once larger data sets are utilized.

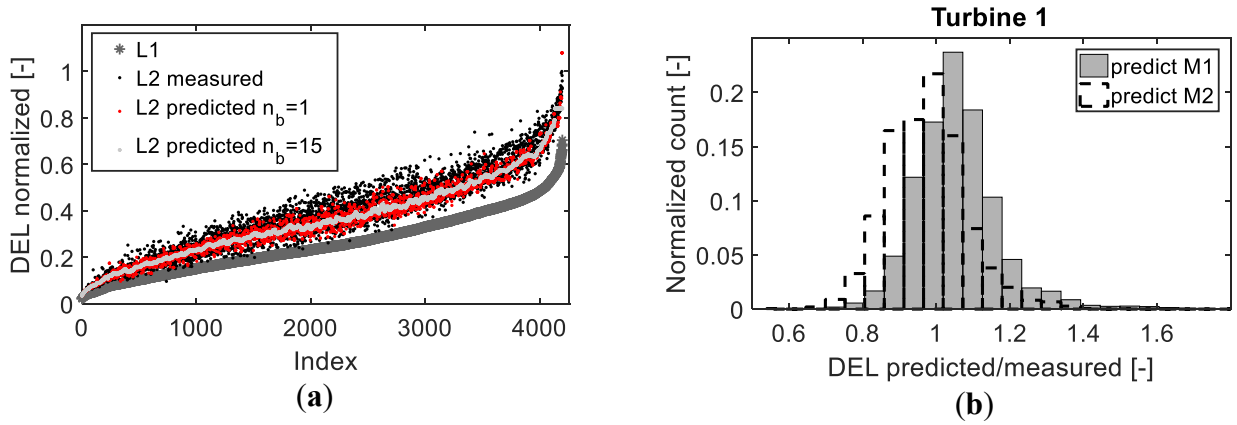

Figure 7. (a) Prediction of DELs from month *M2* (testing data set) with data from month *M1* (training data set) for turbine 1 (case 1). *L1* is the upper and *L2* the lower elevation. DELs are normalized to the maximum of the lower elevation *L2* measured. **(b)** Histogram of data-based extrapolation results for turbine 1 (case 1).

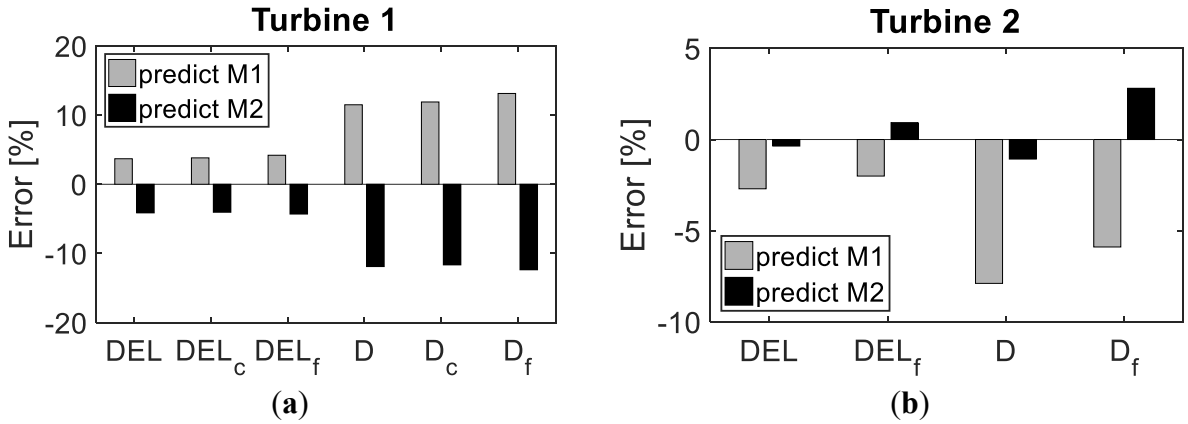

Figure 8. Prediction errors for monthly DELs and monthly damage (D) with and without filtering for produced power recorded by the SCADA system. Index *f* denotes that a filter for produced power is applied (case 2). Index *c* denotes that the data set was cleaned so that only 95% of recorded DELs were used (case 3). **(a)** Results for turbine 1 with strain gauges 15 m apart. **(b)** Results for turbine 2 with strain gauges 25 m apart.

Interestingly, the extrapolation results were better for turbine 2 than for turbine 1, although the strain gauges are located at larger distance. This was unexpected since the extrapolation should be better the closer the sensors are (assuming that there are no local stress effects). It may indicate that the extrapolation is more sensitive to measurement noise than distance between elevations.

3.3. Discussion

The verification study has confirmed that the novel load extrapolation method is applicable to measurement data from two offshore wind monopiles. Prediction errors are in the same order of magnitude compared to results from tests with simulation data-only as performed previously by Ziegler et al [16]. Extrapolations with simulated data, where artificial measurement noise was imposed on the time series, resulted in an error of 4% for estimation of DELs [16]. This accuracy is very promising for fast and cheap evaluation of the loading history of a monopile and thus lifetime extension assessments.

Unfortunately, only two consecutive months of data were available for this study with wave conditions more benign than values used in design. Further work is therefore necessary to address uncertainties arising from variations of weather conditions throughout a year or longer, e.g., how the method performs under more extreme loading conditions. It can be hypothesized that the relationship between measured and predicted fatigue loads becomes more nonlinear under extreme loading conditions, which raises the question if the proposed approach will still result in accurate predictions. In fact, one would expect that linear regression would lead to less accurate results in such situations, whereas the nonlinear k-nearest neighbour algorithm (or a different, nonlinear regression method) would be expected to still deliver relatively accurate results. This is the reason that this paper focusses on prediction with such a nonlinear regression method.

Main limitations of the presented methodology are the accuracy of strain measurements. According to Martinez-Luengo et al [23], strain gauges are a mature technology with easy installation; however, the sensors are not very robust, have a short service life, and the installation is sensitive to misalignments. If strain data from the measured elevation has a large level of noise or includes measurement errors, the extrapolated DEL will also yield unrealistic results. A redundant setup of strain gauges (installed at opposite sides of the circumferential of the structure) helps to assess measurement noise and calibration offsets quickly. In the long-term, reliability of strain gauges might become an issue requiring extrapolation from some (representative) measurement years.

In an application for lifetime extension, the load extrapolation algorithm would need to be trained with aero-hydro-servo-elastic simulations (simulation-based extrapolation, cf. Figure 2) instead of measurement data for elevations without sensors, or if not enough measurement data is available to cover all possible loading conditions (the k-nearest neighbor algorithm cannot extrapolate beyond the range of available training data). This might add additional prediction errors and has to be addressed in future work. The current concept only addresses the extrapolation of load measurements along a single monopile substructure. In large offshore wind farms, only selected wind turbines are typically instrumented with sensors. Future work is necessary to transfer the measured and extrapolated loads to non-instrumented wind turbines in a park.

4. Conclusion and future work

Lifetime extension requires low-cost approaches to assess the remaining useful lifetime of offshore wind monopiles. For this purpose, a novel method to extrapolate loads from one level of strain gauges to the entire monopile is proposed by the authors and verified with measurement data (as far as the limited data allows) in this paper. We conclude that the simple and cheap monitoring concept is able to predict damage equivalent loads at unmeasured elevations with good accuracy. In addition, results showed that the load

extrapolation algorithm is insensitive to the distance between measured elevation and predicted elevation. The verification was performed with measurement data only here. In a next step, training the extrapolation algorithm with aero-hydro-servo-elastic simulations from an updated finite element model should be performed and verified with measurement data. More data, e.g. for at least a whole year, should be obtained to verify the method for the full range of loading conditions. In addition, further work is desirable to improve filtering of measurement data for noise and unphysical recordings if no redundant sensors are available.

Acknowledgement

This project received funding from European Union's Horizon 2020 research and innovation program under the Marie Sklodowska-Curie grant agreement No 642108. We thank the operator for providing measurement data for the study.

References

1. Ho, A.; Mbistrova, A. The European Offshore Wind Industry - Key Trends and Statistics 2016, *Report*, Wind Europe, Brussels, 2017.

2. DNV GL. Lifetime extension of wind turbines. *DNVGL-ST-0262*. 2016.

3. Ziegler, L.; Muskulus, M. Fatigue reassessment for lifetime extension of offshore wind monopile substructures. *Journal of Physics: Conference Series* **2016**, 753(9); IOP Publishing, https://doi.org/10.1088/1742-6596/753/9/092010.

4. Ziegler, L.; Muskulus, M. Lifetime extension of offshore wind monopiles: Assessment process and relevance of fatigue crack inspection. Proceedings of the 12th EAWE PhD Seminar, DTU Lyngby, Denmark; 2016.

5. Zhou, Y. Assessment of bridge remaining fatigue life through field strain measurement. *J Bridge Eng* **2006**, 11(6), https://doi.org/10.1061/(ASCE)1084-0702(2006)11:6(737)

6. Leander, J.; Andersson, A.; Karoumi, R. Monitoring and enhanced fatigue evaluation of a steel railway bridge. *Engineering Structures* **2010**, 32(3), 854-863, https://doi.org/10.1016/j.engstruct.2009.12.011.

7. Frangopol, D.M.; Strauss, A.; Kim, S. Bridge reliability assessment based on monitoring. *Journal of Bridge Engineering* **2008**, 13(3), 258–270, https://doi.org/10.1061/(ASCE)1084-0702(2008)13:3(258).

8. Farreras-Alcover, I.; Chryssanthopoulos, M.K.; Andersen, J.E. Data-based models for fatigue reliability of orthotropic steel bridge decks based on temperature, traffic and strain monitoring. *International Journal of Fatigue* ***2017,*** 95, 104-119, https://doi.org/10.1016/j.ijfatigue.2016.09.019.

9. Pasquier, R; D'Angelo, L; Goulet, JA; Acevedo, C; Nussbaumer A; Smith IF. Measurement, data interpretation, and uncertainty propagation for fatigue assessments of

structures. *Journal of Bridge Engineering* **2016**, 21(5), 04015087, https://doi.org/10.1061/(ASCE)BE.1943-5592.0000861.

10. Hajializadeh, D; Obrien, EJ; O'Connor, AJ. Virtual structural health monitoring and remaining life prediction of steel bridges. *Canadian Journal of Civil Engineering* **2017**, 44(4), 264-273, https://doi.org/10.1139/cjce-2016-0286.

11. Maes, K; Iliopoulos, A; Weijtjens, W; Devriendt, C; Lombaert, G. Dynamic strain estimation for fatigue assessment of an offshore monopile wind turbine using filtering and modal expansion algorithms. *Mechanical Systems and Signal Processing* **2016**, 76, 592-611, https://doi.org/10.1016/j.ymssp.2016.01.004.

12. Iliopoulos, A; Shirzadeh, R; Weijtjens, W; Guillaume, P; Van Hemelrijck, D; Devriendt, C. A modal decomposition and expansion approach for prediction of dynamic responses on a monopile offshore wind turbine using a limited number of vibration sensors. *Mechanical Systems and Signal Processing* **2016**, 68, 84-104, https://doi.org/10.1016/j.ymssp.2015.07.016.

13. Fallais, D.J.M; Voormeeren, S.; Lourens, E. Vibration-based Identification of Hydrodynamic Loads and System Parameters for Offshore Wind Turbine Support Structures. *Energy Procedia* **2016,** 94, 191-198, https://doi.org/ 10.1016/j.egypro.2016.09.222.

14. Smolka, U.; Cheng, P.W. On the design of measurement campaigns for fatigue life monitoring of offshore wind turbines, Proceedings of The Twenty-third International Offshore and Polar Engineering Conference, International Society of Offshore and Polar Engineers, 2013.

15. Cosack, N. Fatigue load monitoring with standard wind turbine signals, PhD thesis, Universität Stuttgart, Germany, 2011.

16. Ziegler, L.; Smolka, U.; Cosack, N; Muskulus, M. Brief communication: Structural monitoring for lifetime extension of offshore wind monopiles: can strain measurements at one level tell us everything?, *Wind Energ. Sci*. **2017**, 2, 469-476, https://doi.org/10.5194/wes-2-469-2017.

17. Vorpahl, F.; Schwarze, H.; Fischer, T.; Seidel, M.; Jonkman, J. Offshore wind turbine environment, loads, simulation, and design. Wiley Interdisciplinary Reviews: Energy and Environment **2013**, 2(5), 548-570.

18. Ziegler, L.; Muskulus, M. Comparing a Fracture Mechanics Model to the SN-Curve Approach for Jacket-Supported Offshore Wind Turbines: Challenges and Opportunities for Lifetime Prediction. ASME. International Conference on Offshore Mechanics and Arctic Engineering, Volume 6: Ocean Space Utilization; Ocean Renewable Energy:V006T09A054. https://doi.org/10.1115/OMAE2016-54915.

19. DNV GL. Support structures for wind turbines. *DNVGL-ST-0126*. 2016.

20. DNV GL. Fatigue design of offshore steel structures. *DNVGL-RP-C203*. 2016.

21. Petersen, C. *Stahlbau.* Springer Fachmedien Wiesbaden, Wiesbaden. 2013.

22. IEC. Wind turbines – part 3: Design requirements for offshore wind turbines. International standard *IEC 61400-3*. Geneva: International Electrotechnical Commission. 2009.

23. Martinez-Luengo, M.; Kolios, A.; Wang, L. Structural health monitoring of offshore wind turbines: A review through the Statistical Pattern Recognition Paradigm, *Renewable and Sustainable Energy Reviews* **2016**, 64, 91-105, https://doi.org/10.1016/j.rser.2016.05.085.